Structural Engineering and Mechanics, Vol. 34, No. 6 (2010) 755-778
DOI: http://dx.doi.org/10.12989/sem.2010.34.6.755

Characterization and modeling of near-fault pulse-like strong ground motion via damage-based critical excitation method

Abbas Moustafa[1] and Izuru Takewaki[2]*

[1]*Department of Civil Engineering, Minia University, Minia 61111, Egypt*
[2]*Department of Urban & Environmental Engineering, Graduate School of Engineering, Kyoto University, Kyotodaigaku-Katsura, Nishikyo-ku, Kyoto 615-8540, Japan*

(Received March 13, 2009, Accepted January 13, 2010)

Abstract. Near-fault ground motion with directivity or fling effects is significantly influenced by the rupture mechanism and substantially different from ordinary records. This class of ground motion has large amplitude and long period, exhibits unusual response spectra shapes, possesses high PGV/PGA and PGD/PGA ratios and is best characterized in the velocity and the displacement time-histories. Such ground motion is also characterized by its energy being contained in a single or very few pulses, thus capable of causing severe damage to the structures. This paper investigates the characteristics of near-fault pulse-like ground motions and their implications on the structural responses using new proposed measures, such as, the effective frequency range, the energy rate (in time and frequency domains) and the damage indices. The paper develops also simple mathematical expressions for modeling this class of ground motion and the associated structural responses, thus eliminating numerical integration of the equations of motion. An optimization technique is also developed by using energy concepts and damage indices for modeling this class of ground motion for inelastic structures at sites having limited earthquake data.

Keywords: near-fault; pulse-like ground motion; frequency content; energy rate; inelastic response; ductility; damage index; critical excitation.

1. Introduction

Resonant or pulse-like (also known as cycloidal pulses or impulse-like) ground motion has been observed in near-fault (also known as near-field or near-source) records with directivity focusing or fling effects. This class of ground motion is significantly influenced by the rupture mechanism, substantially different from ordinary records, and can be characterized by the following tendencies, see, e.g., (Housner and Hudson 1958, Housner and Trifunac 1967, Anderson and Bertero 1987, Hall *et al.* 1995, Heaton *et al.* 1995, Makris 1997, Zhang and Makris 2001, Bray and Rodrigues-Marek 2004, among others): (1) large amplitudes and long period, (2) high PGV/PGA and PGD/PGA ratios, (3) unusual response spectra shapes, and (4) the energy being contained in a single or a few pulses.

Pulse-like ground motions occurring close to urban and metropolitan regions can place severe

*Corresponding author, Professor, E-mail: takewaki@archi.kyoto-u.ac.jp

Table 1 Information on near-fault ground motion (PEER 2005)

Event, station and record	Site condition*	M_W	Source-site Dist. (km)	PGA (g)	PGV (m/s)	PGD (m)	r_1 (s)	r_2 (s^2)	Duration (s)	Intensity (m/s$^{1.5}$)	$\overline{\omega}_{ef}$ **	$\overline{\omega}_s$ ***
1940 El Centro, ELC#9, H180	medium	7.0	12.99	0.31	0.30	0.13	0.10	0.04	40.00	10.64	0.26	0.66
1940 El Centro, ELC#9, H270	medium	7.0	12.99	0.22	0.30	0.24	0.14	0.11	40.00	7.46	0.13	0.70
1966 Parkfield, Chol.#2, C02065	medium	6.1	31.04	0.48	0.75	0.23	0.16	0.05	43.69	11.13	0.17	0.68
1971 San Fernando, LA HW, PCD164	medium	6.6	11.86	0.21	0.19	0.12	0.10	0.06	28.00	4.06	0.16	0.70
1978 Tabas, Tabas, TAB-LN	medium	7.4	55.24	0.84	0.98	0.37	0.12	0.05	32.84	8.49	0.13	0.61
1978 Tabas, Tabas, TAB-TR	medium	7.4	55.24	0.85	1.22	0.95	0.15	0.11	32.84	8.48	0.11	0.62
1979 Imperial Valley, H-AEP045	medium	6.5	2.47	0.33	0.43	0.10	0.13	0.03	11.15	7.15	0.35	0.68
1979 Imperial Valley, H-E06230	medium	6.5	27.47	0.44	1.10	0.66	0.26	0.15	39.04	3.31	0.08	0.76
1981 Westmorland, WSM-090	medium	5.8	7.02	0.37	0.49	0.11	0.14	0.03	40.00	10.96	0.14	0.74
1989 Loma Prieta, LGP000	rock	6.9	18.46	0.56	0.95	0.41	0.17	0.08	24.97	49.12	0.17	0.77
1992 Erzincan, ERZ-NS	medium	6.9	8.97	0.52	0.84	0.27	0.17	0.05	21.31	9.42	0.19	0.89
1992 Landers, LCN-275	rock	7.3	44.02	0.72	0.98	0.70	0.14	0.10	48.13	43.46	0.06	0.61
1992 Landers, JOS-090	stiff	7.3	13.67	0.28	0.43	0.15	0.16	0.06	44.00	14.67	0.17	0.69
1992 Cape Mendocino, CPM000	rock	7.1	10.36	**1.50**	1.27	0.41	0.09	0.03	30.00	27.19	0.16	0.63
1994 Northridge, Rinaldi, RRS228	medium	6.7	10.91	0.84	1.66	0.29	0.20	0.04	14.95	46.03	0.31	0.78
1994 Northridge, Sylmar, SCS052	medium	6.7	13.11	0.61	1.17	0.54	0.20	0.09	40.00	36.42	0.21	0.78
1995 Kobe, Takatori-000	soft	6.9	13.12	0.61	1.27	0.36	0.21	0.06	40.96	54.31	0.17	0.75
1995 Kobe, Takatori-090	soft	6.9	13.12	0.62	1.21	0.33	0.20	0.06	40.96	7.13	0.20	0.72
1995 Kobe, KJM-000	stiff	6.9	18.27	0.82	0.81	0.18	0.10	0.02	48.00	7.24	0.21	0.69
1995 Kobe, KJM-090	stiff	6.9	18.27	0.60	0.74	0.20	0.13	0.03	48.00	5.83	0.21	0.69
1999 Kocaeli, YPT060	medium	7.4	19.30	0.27	0.66	0.57	0.25	0.22	35.00	1.36	0.06	0.85
1999 Chichi, TCU068-N	medium	7.6	47.86	0.46	**2.63**	**4.30**	**0.58**	**0.95**	90.00	20.06	0.02	0.83
1999 Chichi, TCU068-W	medium	7.6	47.86	0.57	1.77	3.24	0.32	0.58	90.00	20.62	0.02	0.87
1999 Chichi, ALS-E	stiff	7.6	37.83	0.18	0.39	0.10	0.22	0.06	59.00	6.00	0.12	0.77
1999 Chichi, TCU078W	medium	7.6	4.96	0.44	0.39	0.31	0.09	0.07	90.00	36.15	0.07	0.73
1999 Chichi, TCU089N	stiff	7.6	7.04	0.25	0.31	0.32	0.13	0.13	79.00	9.64	0.07	0.73
1999 Duze, DZC180	medium	7.1	1.61	0.35	0.60	0.42	0.18	0.12	25.89	16.83	0.09	0.84

*Soft soil: $v_s < 180$ m/s, medium soil: $180 \le v_s < 360$ m/s, stiff soil: $360 \le v_s < 750$ m/s, rock soil: $v_s \ge 750$ m/s
r_1 = PGV/PGA, r_2 = PGD/PGA. **$a = 0.01$, $b = 0.01$. ***$(\Omega_0, \Omega_u) = 2\pi \times (0{,}50)$ rad/s

demands on buildings and other facilities in the near-fault region. The 1923 Kanto earthquake is a striking example of a great earthquake occurring close to a heavily populated city killing more than 140,000 persons (59,000 in Tokyo) and causing property damage of more than $2.0 billion (Hough and Bilham 2006). The 1957 Port Hueneme earthquake of magnitude 4.7 was the first earthquake that consisted of a single pulse (Housner and Hudson 1958). Since the energy was concentrated in one pulse, the damage caused by this earthquake was unusual for a moderate earthquake. Similarly, the 1966 Parkfield earthquake measured 61 m from the source consisted of three pulses (Anderson and Bertero 1987). Near-fault effects have been known for many years and became a focus of research after the 1994 Northridge and the 1995 Kobe earthquakes.

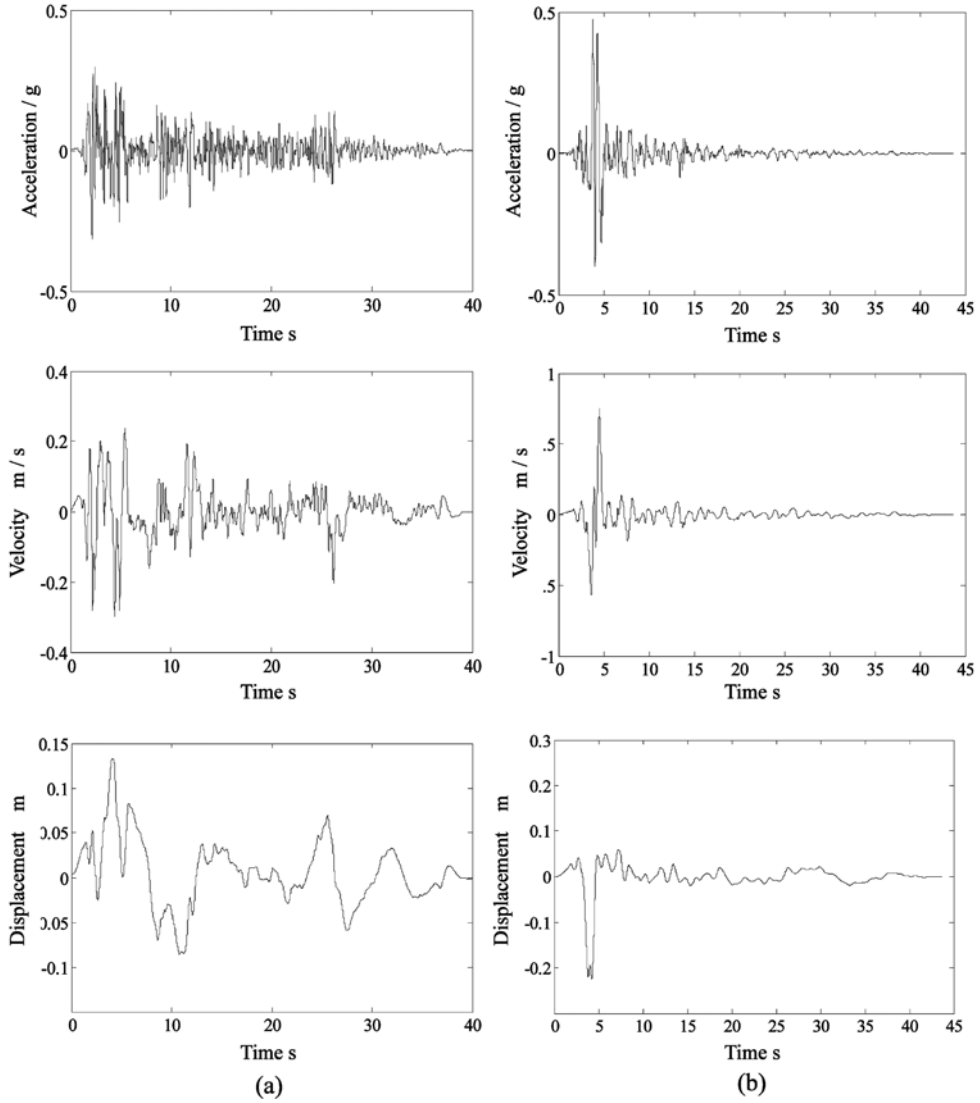

Fig. 1 Near-fault ground motion (a) 1940 El Centro #9, H180, (b) 1966 Parkfield earthquake (Cholame # 2, C02065)

Table 1 lists 27 near-fault records from 15 earthquakes (PEER 2005). Fig. 1 shows the acceleration, velocity and displacement of three pulse-like records and one ordinary record (1940 El Centro) from Table 1. The resonance and large velocity and displacement amplitudes of pulse-like motions are evident from Fig. 1. The 1999 Chichi record exhibits unusual high peak ground velocity and displacement (see Fig. 1(d) and Table 1).

The widespread damage caused to code designed structures during the 1994 Northridge and the 1995 Kobe earthquakes has motivated engineers and researchers for better understanding of near-fault ground motions of impulsive characteristics. Meanwhile, the increasing availability of strong

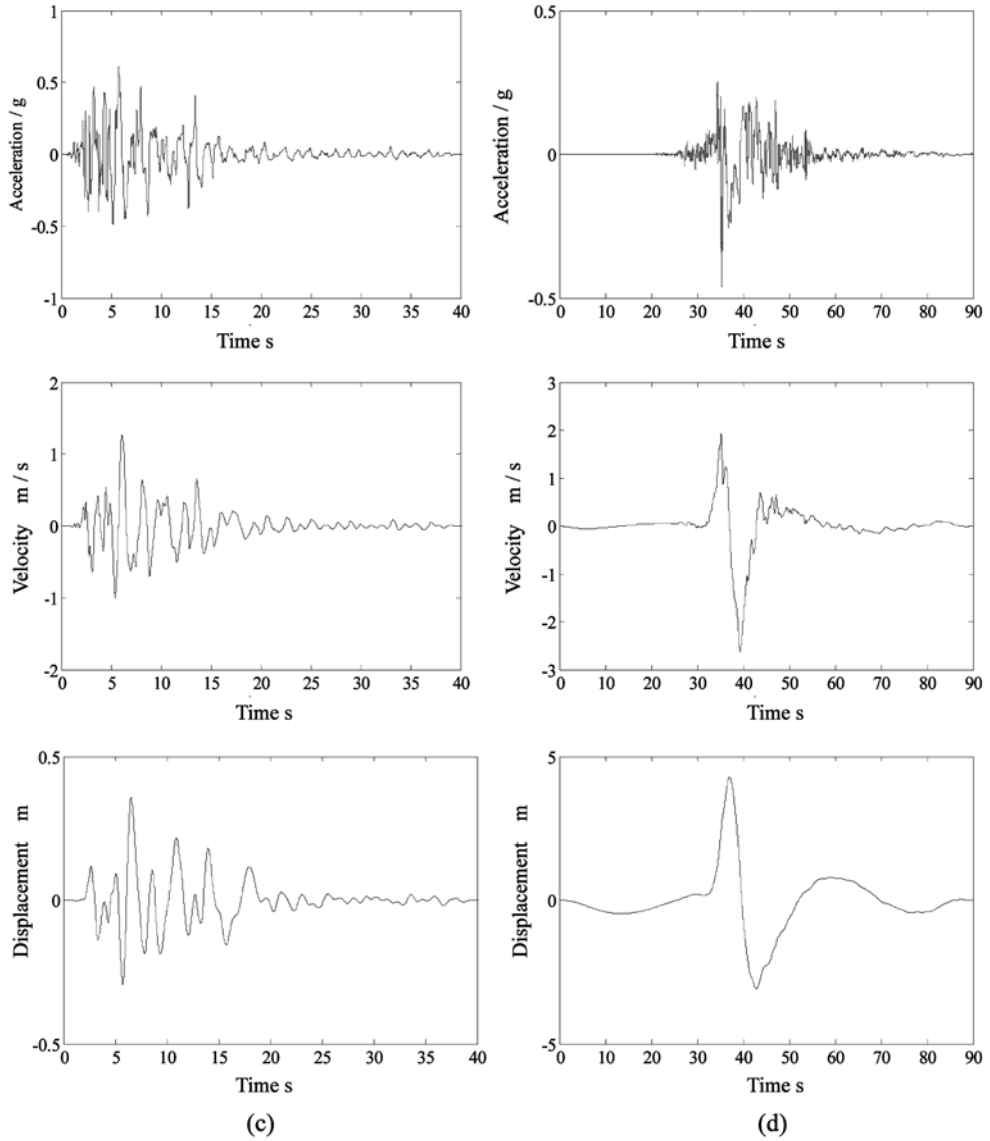

Fig. 1 (continued) Near-fault ground motion (c) The 1995 Kobe earthquake (Takatori, TAK000), (d) The 1999 Chichi earthquake (TCU068-N)

ground motion data (e.g., from Japan, California, Taiwan, Turkey, India and Iran) and the ease in accessing this data facilitate studying this class of ground motions and their effects on man-made structures. With this in mind, the objectives of this paper are: (1) to demonstrate the distinctive features of near-fault pulse-like ground motions and their differences from ordinary records, (2) to investigate the structural performance to this class of ground motion using energy concepts and damage indices, and (3) to provide simple mathematical models for pulse-like ground motion using optimization techniques, energy concepts and damage indices for sites having limited earthquake data. The next section summarizes various measures for characterizing near-fault ground motions.

2. Characterization of near-fault pulse-like ground motion

The characterization of earthquake ground motions and their potential to damage structures can be quantified in terms of measures of the recorded free-field ground motion or in terms of measures that are based on the structure performance during ground shaking as follows:

(1) Free-field measures: These are parameters based on the ground motion records, such as, magnitude, energy, PGA, PGV, PGD, frequency content, duration, epicentral distance, etc. These parameters are independent of the structural properties, and, thus have limited capability in quantifying the earthquake capability to damage the structures.
(2) Elastic response spectra: Examples include the response spectra, the spectrum intensity, and the drift spectra. These parameters do not account for inelastic structural behavior including effects from amplitude and number of cycles of inelastic stress reversals.
(3) Inelastic response spectra: These are generally based on the maximum inelastic response of single-degree-of-freedom (SDOF) structures and include displacement, ductility, interstory drift and design spectra. These parameters do not include effects from the ground motion duration and cumulative energy dissipated by the structure.
(4) Energy spectra: This includes the cumulative energy dissipated by damping and yielding. These parameters include fundamental features of inelastic response and cumulative effects of repeated cycles of inelastic deformation and duration of ground motion. The use of these measures requires normalization with respect to the structure's energy dissipation capacity.
(5) Damage spectra: These measures represent the variation of a damage index versus the structural natural period. Damage indices contain contribution from maximum deformation excursion and cumulative energy dissipated by the structure, and, thus, are robust measures for the earthquake potential to damage the structures.

In this study we utilize the above measures and develop new measures for the frequency content of the ground acceleration to characterize pulse-like strong ground motion for the set of records listed in Table 1. The two horizontal components of the 1940 Imperial Valley earthquake (ordinary records) of M_W = 6.9 are also included in the set of records for comparison.

2.1 Measures based on the recorded free-field ground motion

The distinct pattern of near-fault ground motion can be observed in the time-histories of the ground velocity and displacement, and, also in the large ratios of PGV/PGA and PGD/PGA (see Fig. 1 and Table 1). For instance, pulse-like records exhibit large velocity and displacement amplitudes compared to ordinary records. An example is the TCU068 NS component of the 1999

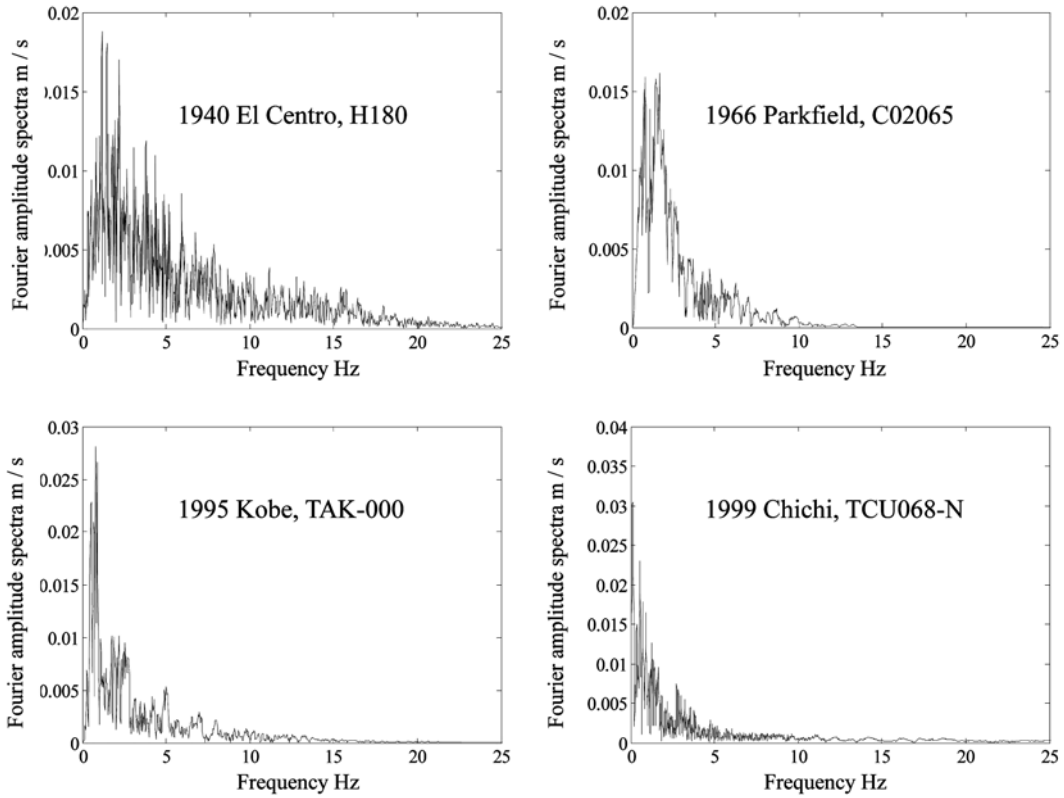

Fig. 2 Fourier amplitude of some of the ground accelerations in Fig. 1

Chichi earthquake. The ratios of PGV/PGA and PGD/PGA are substantially large for these records compared to ordinary records.

Fig. 2 shows the Fourier amplitude spectra for the earthquake accelerations of Fig. 1. Each acceleration record is scaled to unit Arias intensity (Arias 1970). In other words, the square root of the area under the square of the ground acceleration is set to unity. Note that this scaling affects the amplitude of the ground acceleration and does not alter the frequency content. It can be seen that the near-fault records (e.g., 1995 Kobe and 1999 Chichi earthquakes) possess narrow frequency contents compared with the 1940 El Centro records. It is also remarkable that the peak Fourier amplitude of the Kobe and Chichi records are higher than those from ordinary records. We propose a new measure for quantifying the frequency content of the ground acceleration below.

The Arias intensity of the ground acceleration is given as (Arias 1970)

$$E_t = \left[\int_{-\infty}^{\infty} [\ddot{x}_g(\tau)]^2 d\tau \right]^{1/2} \tag{1}$$

Eq. (1) provides a measure of the acceleration energy computed in time domain. Let $\ddot{X}_g(\omega) = \int_{-\infty}^{\infty} \ddot{x}_g(t) e^{-i\omega t} dt$ denotes the Fourier transform of the ground acceleration. Recalling Parseval's theorem expressed by

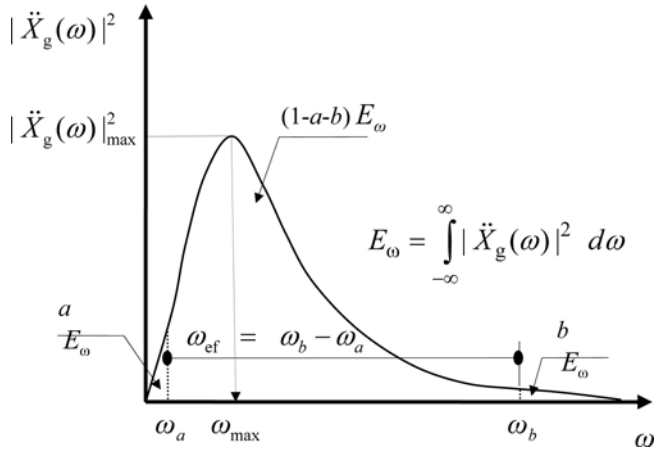

Fig. 3 Measures of frequency bandwidth of recorded ground accelerations

$$\int_{-\infty}^{\infty} [\ddot{x}_g(t)]^2 dt = \frac{1}{2\pi} \int_{-\infty}^{\infty} |\ddot{X}_g(\omega)|^2 d\omega \tag{2}$$

a similar measure can be obtained in frequency domain

$$E_\Omega = \left[\int_{-\infty}^{\infty} |\ddot{X}_g(\omega)|^2 d\omega \right]^{1/2} = \left[\int_{-\infty}^{\infty} \ddot{X}_g(\omega) \ddot{X}_g^*(-\omega) d\omega \right]^{1/2} \tag{3}$$

Herein, $\ddot{X}_g^*(-\omega)$ is the complex conjugate function of $\ddot{X}_g(\omega)$. The new measure for the frequency content of the ground motion proposed in this paper is taken as (ω_a, ω_b). Herein, ω_a and ω_b represent the frequencies at which a and $(1-b)$ times the Fourier energy E_Ω are attained, respectively. Thus, the frequency bandwidth is taken to be given as $\omega_{ef} = \omega_b - \omega_a$ (see Fig. 3). Typical values of a and b can be taken as $a = b = 0.05$ or any reasonable values (e.g., 0.01 or 0). When $a = b = 0.05$, ω_{ef} can be viewed as a measure of the frequencies contributing to the strong phase of the ground motion (Trifunac and Brady 1975). Furthermore, ω_{ef} can be normalized to provide a measure bounded between zero and one

$$\overline{\omega}_{ef} = \frac{\omega_b - \omega_a}{\Omega_u - \Omega_0} \tag{4}$$

The frequency content (Ω_0, Ω_u) is generally in the range of $2\pi \times$ (0,5~50) rad/s depending on the site soil condition and the fault-rupture properties. When $\overline{\omega}_{ef}$ is close to zero, the ground motion resembles the resonance or pulse-like trend. An example of this scenario is a harmonic signal of a single or a few frequencies (e.g., $\ddot{x}_g(t) = A\sin(\omega_g t)$, where A, ω_g are the acceleration amplitude and dominant frequency, respectively). When $\overline{\omega}_{ef}$ is significantly larger than zero, the ground acceleration will be rich in frequencies. The frequency bandwidth of the ground motion can also be quantified based on the random vibration theory as follows

$$\omega_s = \sqrt{\omega_2^2 - \omega_1^2}; \ \omega_i = \int_{-\infty}^{\infty} \omega^i |\ddot{X}_g(\omega)|^i d\omega \Big/ \int_{-\infty}^{\infty} |\ddot{X}_g(\omega)|^2 d\omega \tag{5}$$

where, ω_1 is the central frequency of the ground acceleration and ω_s is the radius of gyration; a

measure of the dispersion of the center of mass of the Fourier spectrum function from the central frequency. This measure is based on the work of Vanmarcke (Vanmarcke 1972, 1976) that he used for quantifying the frequency bandwidth of stationary random processes in terms of the moments of the power spectral density (PSD) function. In this paper, we employ the Fourier spectrum of the ground acceleration instead of the PSD function. ω_s can also be normalized with respect to ω_2 to provide a measure $\overline{\omega}_s$ that is bounded between zero and one.

The numerical values of $\overline{\omega}_{ef}$ and $\overline{\omega}_s$ for the 27 earthquake records of Table 1 are listed in the same table. The parameters a and b are taken as $a = b = 0.01$. The values of $\overline{\omega}_{ef}$ are seen to correlate well with the frequency bandwidth of the ground accelerations. Note that $\overline{\omega}_s$ is inversely proportional to the frequency bandwidth. These results reveal that $\overline{\omega}_{ef}$ is an accurate descriptor for the frequency content of the ground acceleration.

As is well known, the energy of the ground acceleration represents an important parameter for characterizing earthquake ground motions (Housner 1970, Arias 1970, Trifunac and Brady 1975, Housner and Jennings 1977). The expressions of the acceleration energy in time and frequency domains are given by Eqs. (1) and (3), respectively. The time and frequency variations of the energy of the ground motion can be useful indicators of the earthquake potential to damage structures. For instance, near-fault ground motion can cause severe damage to structures due to the large input energy to the structure. This feature can be captured by examining the time variation of the acceleration energy and the relation between the structure fundamental frequency and the dominant frequency of the ground motion (Housner 1970, Takewaki 2004). The computation of the energy of the ground motion in the frequency domain is essential for this purpose since it reflects the acceleration energy at various frequencies. Therefore, we use two energy measures for characterizing the earthquake characteristics. The first measure is the energy rate in time domain which represents the instantaneous incremental energy of the ground motion in time domain per unit time. The second measure is the incremental energy of the ground motion in frequency domain per unit frequency. These measures are given as

$$\overline{E}_t(t_i) = \frac{E_t(t_{i+1}) - E_t(t_i)}{t_{i+1} - t_i} = \frac{\Delta E_t(t_i)}{\Delta t_i}; \quad \overline{E}_\Omega(\omega_i) = \frac{E_\Omega(\omega_{i+1}) - E_\Omega(\omega_i)}{\omega_{i+1} - \omega_i} = \frac{\Delta E_\Omega(\omega_i)}{\Delta \omega_i} \tag{6a,b}$$

where

$$E_t(t) = \left[\int_{-\infty}^{t} |\ddot{x}_g(\tau)|^2 d\tau\right]^{1/2}; \quad E_\Omega(\omega) = \left[2\int_{0}^{\omega} |\ddot{X}_g(\gamma)|^2 d\gamma\right]^{1/2} \tag{7a,b}$$

Trifunac and Brady (1975) developed an energy measure for the ground acceleration by normalizing the energy with respect to the total duration of the ground motion. Note that $\overline{E}_t(t)$ provides a robust measure of the acceleration energy at discrete time instants.

The plots of the two measures of Eq. (6) for the records in Fig. 1 are shown in Figs. 4(b) and 5(b). Figs. 4(a) and 5(a) depict the plots of the energies given by Eq. (7). Note that all records are normalized to unit Arias intensity. The effectiveness of the energy measures $\overline{E}_t(t)$ and $\overline{E}_\Omega(\omega)$ in characterizing pulse-like records is evident from the plots shown in Figs. 4 and 5. For instance, the Chichi record has most of its energy concentrated at about 38 s. In frequency domain, the energies of the Kobe and Chichi records are contained in narrow frequency range. It is also seen that the peak amplitude of the Chichi and Kobe records are substantially higher than other records. It is believed that the measures $\overline{\omega}_{ef}$, $\overline{E}_t(t)$ and $\overline{E}_\Omega(\omega)$ provide important information on the nature of

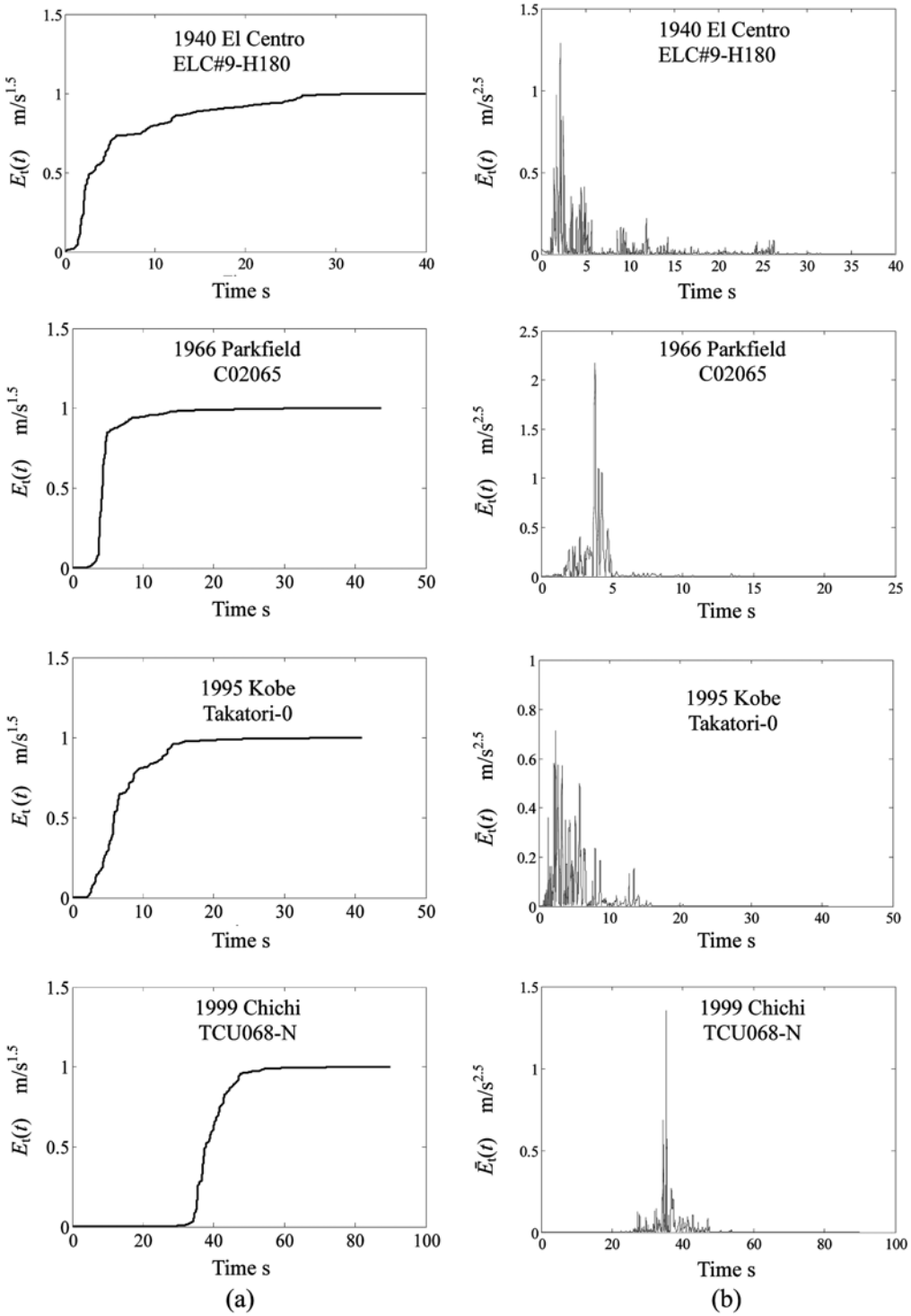

Fig. 4 Energy and energy rate in time domain

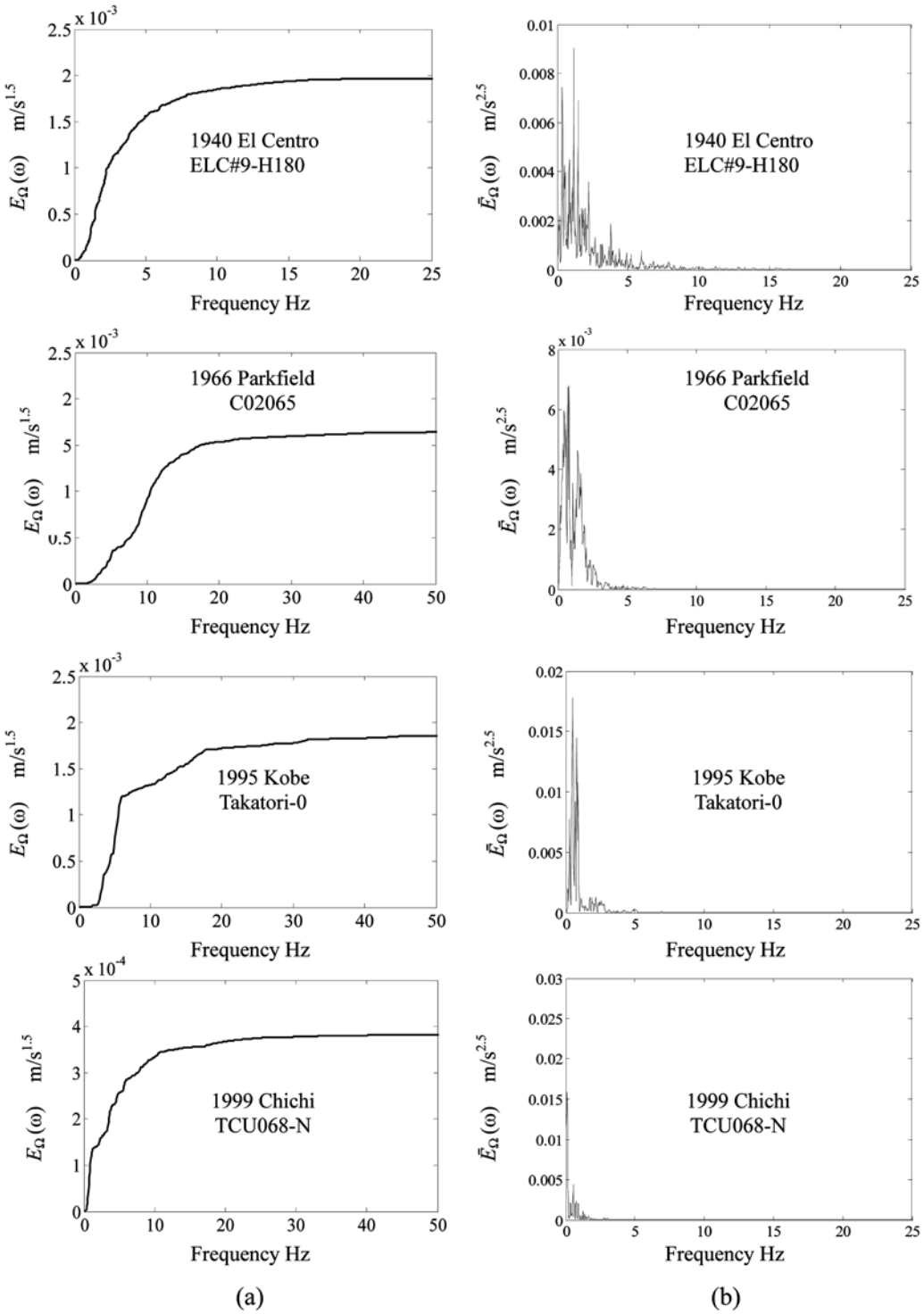

Fig. 5 Energy and energy rate in frequency domain

the ground motion. However, the use of these measures alone for quantifying possible damage of the structure without the inclusion of the structure parameters is inadequate. The next section tackles this limitation by considering measures based on the structural responses.

2.2 Measures based on the structural response

Figs. 6(a) and 6(b) depict the elastic and inelastic response spectra for the records shown in Fig. 1. These plots represent the maximum elastic and inelastic pseudo velocity of the SDOF system versus the natural period, respectively. A viscous damping model with damping ratio of 0.05 is adopted for elastic and inelastic spectra. For the inelastic case, the material nonlinearity is modeled using an elastic-plastic force-deformation law. The yield displacement and strength are taken as x_y = 0.10 m and f_y = 10^4 N. All records are normalized to 0.30 g peak ground acceleration. The significant differences of maximum responses of pulse-like records from ordinary records are remarkable. The Kobe and Chichi records produce significantly higher response spectra compared to ordinary records.

The energy spectrum of the ground acceleration represents the plot of the maximum energy versus

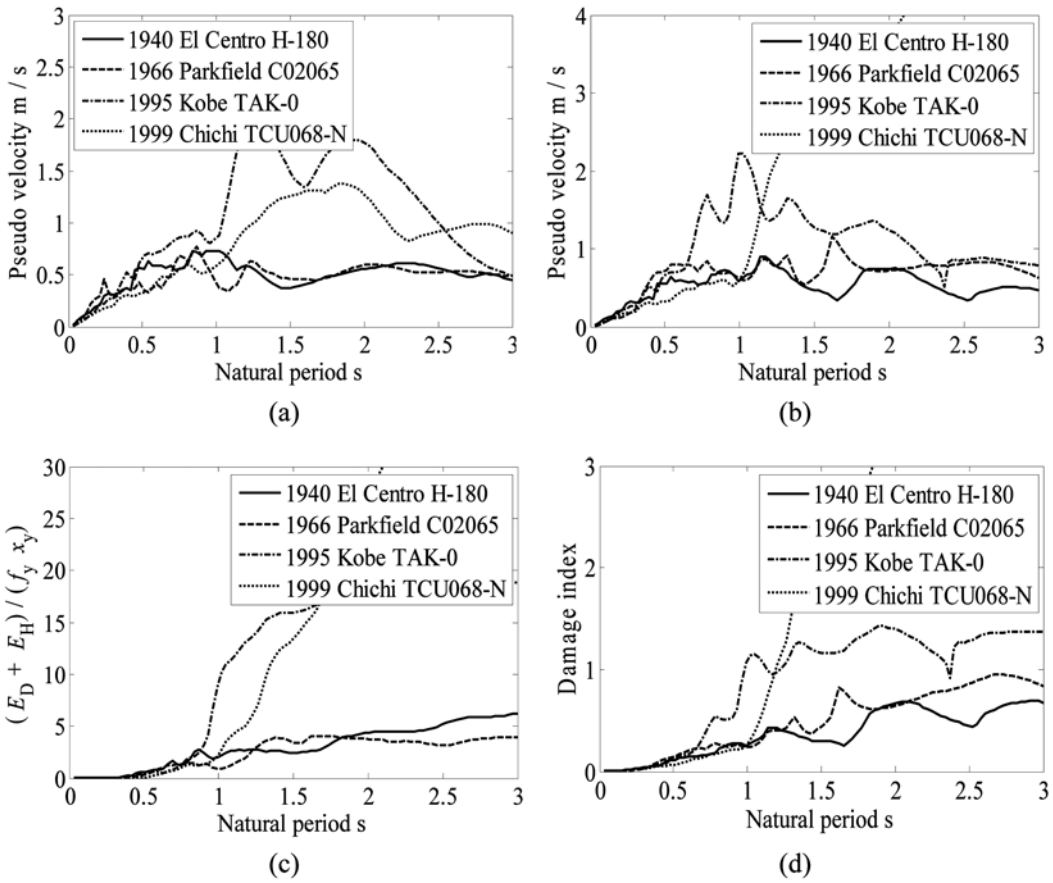

Fig. 6 Pseudo velocity spectra (a) Elastic spectra, (b) Inelastic spectra, (c) Energy spectra, (d) Damage spectra

the natural period. To do this, we consider the equation of motion of an elastic-plastic SDOF system driven by a single component of ground acceleration $\ddot{x}_g(t)$

$$m\ddot{x}(t) + c\dot{x}(t) + f_s(t) = -m\ddot{x}_g(t) \tag{8}$$

where m and c are the mass and damping coefficient of the structure and $f_s(t)$ is the hysteretic restoring force. Integrating Eq. (8), we get (Zahra and Hall 1984, Akiyama 1985, Uang and Bertero 1990, Chai and Fajfar 2000, Takewaki 2004, Abbas 2006, Moustafa 2009)

$$E_K + E_D + E_S = E_I \tag{9}$$

where E_K, E_D, E_S, E_I are the relative kinetic energy, the energy absorbed by damping, the strain energy and the earthquake input energy to the structure, respectively. $E_K(t) = m\dot{x}^2(t)/2$ and $E_S(t)$ is composed of cumulative unrecoverable hysteretic energy $E_H(t)$ and elastic recoverable energy $E_e(t) = kx^2(t)/2$, where k is the initial stiffness.

We construct the dissipated energy spectra $(E_D + E_H)$ for the acceleration records of Fig. 1. These results are presented in Fig. 6(c). The distinct differences for the energy spectra of pulse-like records are evident. The pulse-like records are seen to produce higher energy ordinates than ordinary records.

Structural damage under strong ground motion occurs not only due to the maximum deformation or ductility but also due to the hysteretic cumulative energy dissipated by the structure. The literature on structural damage measures of buildings under strong ground motion is vast (Powel and Allahabadi 1988, Cosenza *et al.* 1993, Ghobara *et al.* 1999). Damage indices are based on either a single or combination of structural response parameters. Measures that are based on a single response parameter, such as, the ultimate ductility or the maximum energy dissipated during the ground shaking do not incorporate information on how the earthquake input energy is imparted on the structure nor how this energy is dissipated. The definition of the structural damage in terms of a single response parameter is thus inadequate. Damage indices can be established by comparing the response parameters demanded by the earthquake with the structural capacities. The damage index developed by Park and co-workers is the most commonly used damage index due to its simplicity and extensive experimental calibration with field observations in earthquakes, and is given as (Park *et al.* 1985)

$$DI_{PA} = \frac{x_{\max}}{x_u} + \lambda\frac{E_H}{f_y x_u} = \frac{\mu_{\max}}{\mu_u} + \lambda\frac{E_H}{f_y x_y \mu_u} \tag{10}$$

Here, $x_{\max}, E_H$ are the maximum absolute displacement and maximum dissipated hysteretic energy under the earthquake. μ_u is the ultimate yield ductility capacity under monotonic loading and λ is a positive constant that weights the effect of cyclic loading on structural damage. The state of the structural damage is defined as:

(a) Repairable damage, when $DI_{PA} < 0.40$,

(b) Damaged beyond repair, when $0.40 \le DI_{PA} < 1.0$, and

(c) Total or complete collapse, when $DI_{PA} \ge 1.0$.

These criteria are based on calibration of DI_{PA} against experimental results and field observations in earthquakes (Park *et al.* 1985). Eq. (10) reveals that both maximum ductility and hysteretic energy dissipation contribute to the structural damage during ground motion. Herein, damage is expressed as a linear combination of the damage caused by excessive deformation and that contributed by repeated cyclic loading effect. Note that the quantities $x_{\max}, E_H$ depend on the

loading history while the quantities λ, x_u, f_y are determined from experimental tests. The numerical results on DI_{PA} are provided in Fig. 6(d). Herein, μ_u is taken as 6 and $\lambda = 0.15$. From the numerical results, it is evident that pulse-like records produce more damage than ordinary records for structures having natural period greater than 0.70 s.

This section demonstrated the characterization of near-field ground motions using measures that are based on the recorded free-field ground motion and those that are based on the structural responses and damage indices. It has been shown that near-fault pulse-like earthquakes possess distinctive features compared with ordinary records, and, also produce large structural responses and damage indices. The next section provides simple analytical expressions for modeling near-fault pulse-like earthquakes.

3. Modeling near-fault pulse-like ground motion

As noted in the introduction section, real recorded ground motions exhibit the resonance nature when the energy of the earthquake ground motion is concentrated in a narrow frequency range. The method of critical excitation may provide a useful tool for modeling pulse-like or resonant ground motion for a given structure (Takewaki 2002, 2006, 2007, Abbas and Manohar 2002, 2007, Abbas 2006). The damage caused by critical ground motions can be significantly larger than those from ordinary ground motion since such ground motion is tailor-made to produce the maximum response. In this section, we construct simple analytical representation of this class of ground motion using optimization techniques and provide simple procedures for solving the optimization problem. These simple analytical expressions can be easily used by the structural engineer to assess the structural safety without numerical integration of the equation of motion to obtain the structural response.

3.1 Representation of pulse-like ground motion using trigonometric functions

A simple functional representation of pulse-like ground motion can be expressed as

$$\begin{aligned} \ddot{x}_g(t) &= A\sin(\omega_p t) \\ \dot{x}_g(t) &= A[1-\cos(\omega_p t)]/\omega_p \\ x_g(t) &= A[t-\sin(\omega_p t)/\omega_p]/\omega_p;\ 0 < t \le T_p = 2\pi/\omega_p \end{aligned} \tag{11}$$

where A is a constant representing the acceleration amplitude and ω_p is the pulse frequency of the ground motion.

This representation has been used earlier for modeling near-fault pulse-like ground motions (Makris 1997). Makris uses the velocity record to derive the pulse frequency ω_p and the acceleration amplitude as $A = (\omega_p \dot{x}_{p_{\max}})/2$. An improved analytical model was developed by He and Agrawal (2008) in which the velocity pulse is represented as a sinusoidal function modulated by an exponential decaying envelope function, given as

$$\dot{x}_g(t) = Ct^n e^{-at}\sin(\omega_p t + \upsilon); \quad t \ge t_0 \tag{12}$$

Herein, ω_p is the pulse frequency, C is an amplitude scaling factor, υ is a phase angle, a is a constant that controls the modulation function, n is a non-negative integer parameter controlling the

skewness of the pulse envelope in time and t_0 is the starting time point of the pulse. These authors derived the analytical expressions for the acceleration and displacement and also for the displacement response of SDOF systems. This model is used for performance-based seismic passive energy dissipation of structures (Tan *et al.* 2005).

In this section, we model resonant or pulse-like ground motion for linear structures. Thus, the parameters ω_p and A of the ground motion are computed by optimization techniques so that the structural response is maximized. Considering the ground motion to be given by Eq. (11), assuming linear elastic behavior and considering zero initial conditions, the displacement response of the SDOF structure can be shown to be given as

$$x(t) = \frac{-mA}{k\sqrt{(1-r^2)^2 + 4\eta^2 r^2}} \sin(\omega_p t - \theta); \quad \theta = \tan^{-1}\left(\frac{2\eta r}{1-r^2}\right) \tag{13}$$

where, r is the ratio of the pulse frequency ω_p and the structure natural frequency ω_n, θ is a phase angle and η is the damping ratio. Hence, the displacement response is given in a closed-form and thus numerical integration of the equation of motion is eliminated. Additionally, the errors associated with the numerical integration are also eliminated.

It can be shown that the resonance of the displacement, velocity and acceleration responses occur at $\omega_n\sqrt{1-2\eta^2}$, ω_n, $\omega_n/\sqrt{1-2\eta^2}$, respectively. For viscous damping model of η = 0.03, these values are $0.9991\omega_n$, ω_n, $1.0009\omega_n$, respectively. Similarly, the resonant frequencies for η = 0.05 are $0.9975\omega_n$, ω_n, $1.0025\omega_n$. Thus, for practical applications the resonance frequency can be taken equal to ω_n.

The representation of the ground motion developed here can be utilized for preliminary analysis and design of structures. The optimization problem is solved in two steps. First, the dominant frequency of the ground motion is taken to coincide with the structure natural frequency. Subsequently, the acceleration amplitude is determined so that the structure response is maximized subject to predefined constraints. These procedures are demonstrated below.

3.1.1 Energy constraint

Arias intensity is recognized as the most commonly used measure of earthquake energy (Arias 1970). Mathematically, this constraint is given as (see Eq. (1))

$$I_A = \left[\int_0^\infty [\ddot{x}_g(t)]^2 dt\right]^{1/2} \tag{14}$$

Making use of Eq. (11), the parameter A can be shown to be given as

$$A = I_A / \sqrt{\int_0^\infty [\sin(\omega_p t)]^2 dt} \tag{15}$$

Thus, the problem reduces to computing the value of the parameter A from the above equation while the pulse frequency is taken to coincide with the structure fundamental frequency.

3.1.2 PGV constraint

In earlier works, the parameters of the pulse model are estimated so that the model possesses the

pulse frequency and peak velocity amplitude observed in previous records. Implicit constraints on the peak values of acceleration and displacement and the ground motion energy are automatically implemented due to the closed-form representation adopted (Moustafa 2010). Here, $\dot{x}_g(t)$ is explicitly constrained to its peak value N, leading to

$$A = \omega_p N / \left|1 - \cos(\omega_p t)\right|_{\max} \tag{16}$$

Thus, the problem reduces to finding the value of the parameter A from Eq. (16). The velocity constraint is known to be more effective than the acceleration constraint (Housner 1970).

The model considered here is referred to as Model I in the numerical analysis. The representation of pulse-like ground motion presented above does not account for the nonstationarity of the ground motion. The next section tackles this limitation.

3.2 Representation of pulse-like ground motion using trigonometric functions modulated by envelope function

The nonstationarity of the ground motion can be accounted for by modulating the sine signal of Eq. (11) with an envelope function as follows

$$\ddot{x}_g(t) = e(t) \qquad \ddot{u}_g(t) = A[\exp(-\alpha t) - \exp(-\beta t)]\sin(\omega_p t) \tag{17}$$

where the parameters α and β control the nonstationarity of the ground acceleration. These parameters can be calculated so that they match the nonstationarity trend of past recorded ground accelerations (Takewaki 2002, 2006, 2007, Abbas and Manohar 2002, 2007, Abbas 2006). The displacement response of the SDOF structure can be shown to be given as

$$x(t) = [B_\alpha \exp(-\alpha t) + B_\beta \exp(-\beta t)]\cos(\omega_p t) + [D_\alpha \exp(-\alpha t) + D_\beta \exp(-\beta t)]\sin(\omega_p t) \tag{18}$$

where

$$\begin{aligned} B_\alpha &= \frac{-2A\,\omega_p(\alpha - \eta\omega_n)}{4\omega_p^2(\alpha - \eta\omega_n)^2 + (\alpha^2 - \omega_p^2 - 2\eta\omega_n\alpha + \omega_n^2)^2} \\ D_\alpha &= \frac{-A(\alpha^2 - \omega_p^2 - 2\eta\omega_n\alpha + \omega_n^2)^2}{4\omega_p^2(\alpha - \eta\omega_n)^2 + (\alpha^2 - \omega_p^2 - 2\eta\omega_n\alpha + \omega_n^2)^2} \end{aligned} \tag{19}$$

The parameters B_β, D_β can be obtained from the above expressions by replacing α with β. The advantages of this representation are (1) elimination of the numerical integration in calculating the structural response and also the error involved in the numerical integration, (2) the exclusion of using nonlinear optimization technique. The model considered here is referred to as Model II in the numerical analysis.

The numerical results for Models I and II are shown in Table 3. Herein, the energy and PGV constraints are taken as 3.26 m/s$^{1.5}$ and 0.30 m/s, respectively. These values are specified to reflect the intensity and PGV of the 1940 El Centro NS record. The elastic and elastic-plastic responses of the same structure to El Centro 1940 NS component are also included in Table 3. The parameters of the elastic-plastic structure are taken as given in Section 2.2. It is observed that the energy constraint (case 1) provides realistic response quantities compared with those produced with the

PGV constraint (case 2). It is also remarkable that the elastic linear model is not sufficient especially when dealing with extreme loads of pulse-like trend. The next section accounts for inelastic structural behavior in modeling pulse-like ground motions.

4. Damage-based critical earthquake ground motion for inelastic structures

4.1 Problem statement

As seen in the introduction and the previous sections, ground motions of near-fault regions affected by directivity focusing or fling effects possess a pulse-like trend. Thus, it is possible that the dominant frequency of the ground motion coincides with the structure fundamental natural frequency. In such case, the ground motion is termed *critical* excitation and produces the largest response in the structure. See, for example (Takewaki 2002, 2006, 2007, Abbas and Manohar 2002, 2007, Abbas 2006) for a review of previous works on this topic. The use of the critical excitation method is generally associated with safety assessment of important structures to be constructed in seismically active regions having limited earthquake data. The method provides an answer to the question on the worst case scenario that can happen to the structure which represents one of the main concerns for structural engineers. The method relies on the high uncertainty associated with earthquake occurrence. Given the importance of including nonlinear structural behavior, this section models pulse-like ground motions for inelastic structures.

Unlike earlier work in which the critical earthquake is taken as the excitation that produces the maximum response, we develop earthquake loads that cause the maximum damage in the structure using energy concepts and damage indices. The ground acceleration is represented as

$$\ddot{x}_g(t) = e(t)\sum_{i=1}^{N_f} R_i \cos(\omega_i t - \phi_i) = A_0[\exp(-\alpha t) - \exp(-\beta t)]\sum_{i=1}^{N_f} R_i \cos(\omega_i t - \phi_i) \tag{20}$$

Here, A_0 is a scaling constant and the parameters α and β impart the transient trend to $\ddot{x}_g(t)$. R_i and ϕ_i are $2N_f$ unknown amplitudes and phase angles, respectively, and ω_i, $i = 1, 2, \ldots, N_f$ are the frequencies presented in the ground acceleration that are selected to span satisfactorily the frequency content of $\ddot{x}_g(t)$. In constructing critical seismic inputs, the envelope function is taken to be known. The information on energy E, peak ground acceleration (PGA) M_1, peak ground velocity (PGV) M_2, and peak ground displacement (PGD) M_3 are also assumed to be available. This enables defining the following constraints (Abbas and Manohar 2002, Abbas 2006)

$$\begin{aligned}
\left[\int_0^{\infty} [\ddot{x}_g(t)]^2 dt\right] &\le E \\
\max_{0<t<\infty} |\ddot{x}_g(t)| &\le M_1 \\
\max_{0<t<\infty} |\dot{x}_g(t)| &\le M_2 \\
\max_{0<t<\infty} |x_g(t)| &\le M_3 \\
M_5(\omega) \le |\ddot{X}_g(\omega)| &\le M_4(\omega)
\end{aligned} \tag{21}$$

Here $\ddot{X}_g(\omega)$ is the Fourier transform of $\ddot{x}_g(t)$. From Eq. (20), the constraints of Eq. (21) can be expressed in terms of the unknown variables R_i, ϕ_i, $i = 1, 2, \ldots, N_f$ as follows

$$\left[A_0^2 \sum_{m=1}^{N_f}\sum_{n=1}^{N_f} R_m R_n \int_0^{\infty} [\exp(-\alpha t) - \exp(-\beta t)]^2 \cos(\omega_m t - \phi_m)\cos(\omega_n t - \phi_n) dt\right]^{1/2} \le E$$

$$\max_{0<t<\infty}\left|A_0[\exp(-\alpha t) - \exp(-\beta t)]\sum_{n=1}^{N_f} R_n \cos(\omega_n t - \phi_n)\right| \le M_1$$

$$\max_{0<t<\infty}\left|A_0 \sum_{n=1}^{N_f}\int_0^t R_n[\exp(-\alpha\tau) - \exp(-\beta\tau)]\cos(\omega_n\tau - \phi_n)d\tau - \right.$$

$$\left. A_0 \sum_{n=1}^{N_f}\int_0^{\infty} R_n[\exp(-\alpha\tau) - \exp(-\beta\tau)]\cos(\omega_n\tau - \phi_n)d\tau\right| \le M_2$$

$$\max_{0<t<\infty}\left|A_0 \sum_{n=1}^{N_f}\int_0^t R_n[\exp(-\alpha\tau) - \exp(-\beta\tau)](t-\tau)\cos(\omega_n\tau - \phi_n)d\tau - \right.$$

$$\left. A_0 t\sum_{n=1}^{N_f}\int_0^{\infty} R_n[\exp(-\alpha\tau) - \exp(-\beta\tau)]\cos(\omega_n\tau - \phi_n)d\tau\right| \le M_3$$

$$M_5(\omega) \le \left|A_0 \sum_{n=1}^{N_f}\int_0^{\infty} R_n\{\exp[-(\alpha + i\omega)t] - \exp[-(\beta + i\omega)t]\}\cos(\omega_n\tau - \phi_n)dt\right| \le M_4(\omega) \qquad (22)$$

where $i = \sqrt{-1}$. The bounds $M_4(\omega)$ and $M_5(\omega)$ aim to replicate the Fourier spectra of past records on the critical ground acceleration (Shinozuka 1970, Takewaki 2001) and are given as

$$M_4(\omega) = E \max_{1 \le i \le N_r}\left|\overline{V}_{g_i}(\omega)\right|; \quad M_5(\omega) = E \max_{1 \le i \le N_r}\left|\overline{V}_{g_i}(\omega)\right| \qquad (23)$$

The function $\overline{V}_{g_i}(\omega)$, $i = 1, 2, \ldots, N_r$ denotes the Fourier transform of the ith normalized accelerogram $\overline{v}_{g_i}(\omega)$ computed using the Fast Fourier Transform.

Therefore, the problem of deriving critical earthquake loads can be posed as determining the variables $\mathbf{y} = \{R_1, R_2, \ldots, R_{N_f}, \phi_1, \phi_2, \ldots, \phi_{N_f}\}^T$ such that DI_{PA} (Eq. (10)) is maximized subject to the constraints of Eq. (22).

It may be emphasized that, the ground energy rate is more effective than the energy constraint in influencing the structural responses. A few authors have confirmed the effectiveness of the energy rate of the ground motion in producing larger structural responses (Trifunac 2005, 2008). Note, however, that the energy of the ground motion indicates the earthquake magnitude and can be easily estimated from the time histories of the ground motion. The energy rate of the ground motion, on the other hand, is a time-dependent function. Constraining the energy rate of the ground motion requires imposing this constraint at discrete points of time which will increase the computations. This constraint can be implemented in the same way the Fourier amplitude spectra constraints have been imposed (see Eqs. (21) and (22)). An alternative is to derive the critical ground velocity by maximizing the energy rate of the ground motion. Takewaki (2006) has considered the input energy rate to the structure in modeling the critical earthquake loads.

4.2 Solution procedures

This nonlinear constrained optimization problem is solved using the sequential quadratic programming (SQP) method (Arora 2004). The following convergence criteria are adopted

$$|f_j - f_{j-1}| \le \varepsilon_1; \quad |y_{i,j} - y_{i,j-1}| \le \varepsilon_2 \tag{24}$$

Herein f_j is the objective function at the jth iteration, $y_{i,j}$ is the ith optimization variable at the jth iteration and $\varepsilon_1, \varepsilon_2$ are small quantities to be specified. The structural inelastic deformation is estimated by solving the incremental form of the equation of motion (Abbas 2006). In distributing the frequencies of Eq. (20), it was found advantageous to place more frequencies within the half bandwidth of the natural frequency of the elastic structure and to select one of these frequencies to coincide exactly with this frequency. This was seen to enable the energy of the ground motion to get distributed around the structure fundamental frequency and to facilitate rapid convergence of the optimization solution. In the numerical analyses, several initial guess were examined and it was found that the optimization converges to the same optimal solution.

It may be emphasized that the quantities $\mu(t) = u_{\max}/u_y$ and $E_H(t)$ do not reach their respective maxima at the same time. Thus, the optimization is solved at discrete time instants and the optimal solution $\mathbf{y}^* = \{R_1^*, R_2^*, \ldots, R_{N_f}^*, \phi_1^*, \phi_2^*, \ldots, \phi_{N_f}^*\}^T$ is the one that produces the maximum DI_{PA} across all time points. The critical earthquake loads are characterized by the accelerations and associated damage indices, inelastic deformations and energy dissipated by the structure. This model is referred to as Model III in the numerical analysis.

4.3 Numerical example

Consider an elastic-plastic SDOF building frame with mass $= 9 \times 10^3$ kg, initial stiffness $k = 1.49 \times 10^5$ N/m and viscous damping model of 0.03 damping ratio. The initial natural frequency is about 4.10 rad/s and the yield force $f_y = 10^4$ N and the yield displacement $u_y = 0.07$ m. The structure is assumed to start from rest.

The constraint quantities are taken as $E = 4.17$ m/s$^{1.5}$, $M_1 = 4.63$ m/s^2 (0.47 g), $M_2 = 0.60$ m/s and $M_3 = 0.15$ m. The envelope parameters are taken as $A_0 = 2.17$, $\alpha = 0.13$, and $\beta = 0.50$. The upper and lower constraints on the Fourier spectra are computed from the set of past records in Table 1 measured at medium soil. The convergence limits $\varepsilon_1, \varepsilon_2$ are taken as 10^{-6}. The frequency content of $\ddot{x}_g(t)$ is taken as $2\pi \times (0\sim25)$ rad/s.

The nonlinear constrained optimization problem is tackled using the SQP method through the Matlab optimization toolbox (Caleman *et al.* 1999). To select the number of frequency terms N_f, a parametric study was carried out and $N_f = 51$ was found to give satisfactory results.

Table 2 Nomenclature of constraint scenarios for Models I, II and III

Case	Models I and II	Model III
1	Energy	Energy and PGA
2	PGV	Energy, PGA, PGV and PGD
3	-	Energy, PGA and UBFS
4	-	Energy, PGA, UBFS and LBFS

UBFS: upper bound of Fourier spectrum, LBFS: lower bound of Fourier spectrum

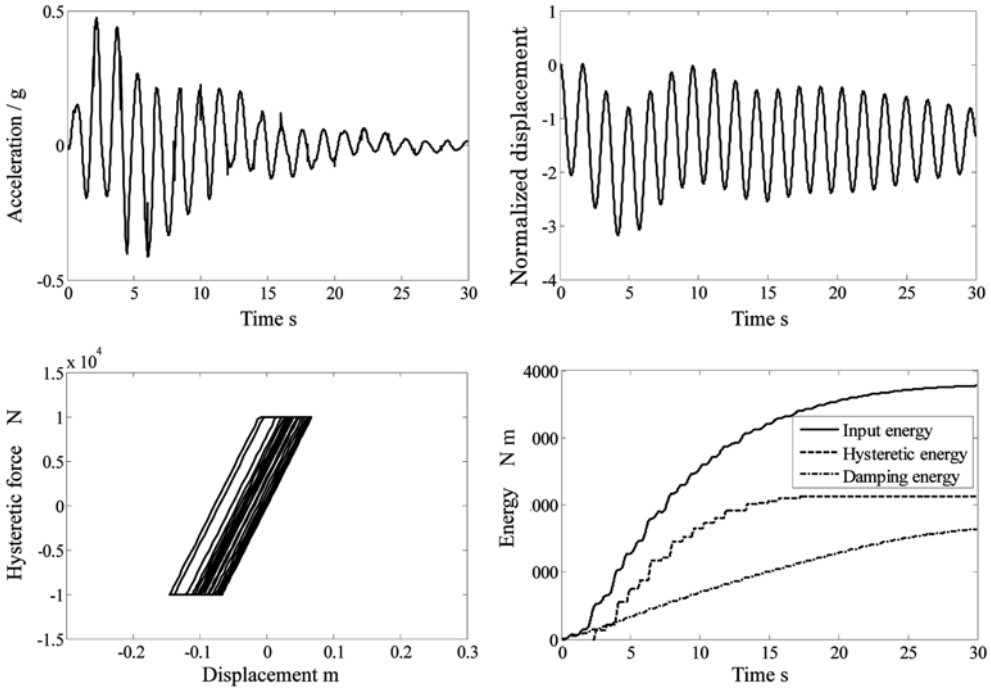

Fig. 7 Critical earthquake accelerations and associated critical responses for case 1

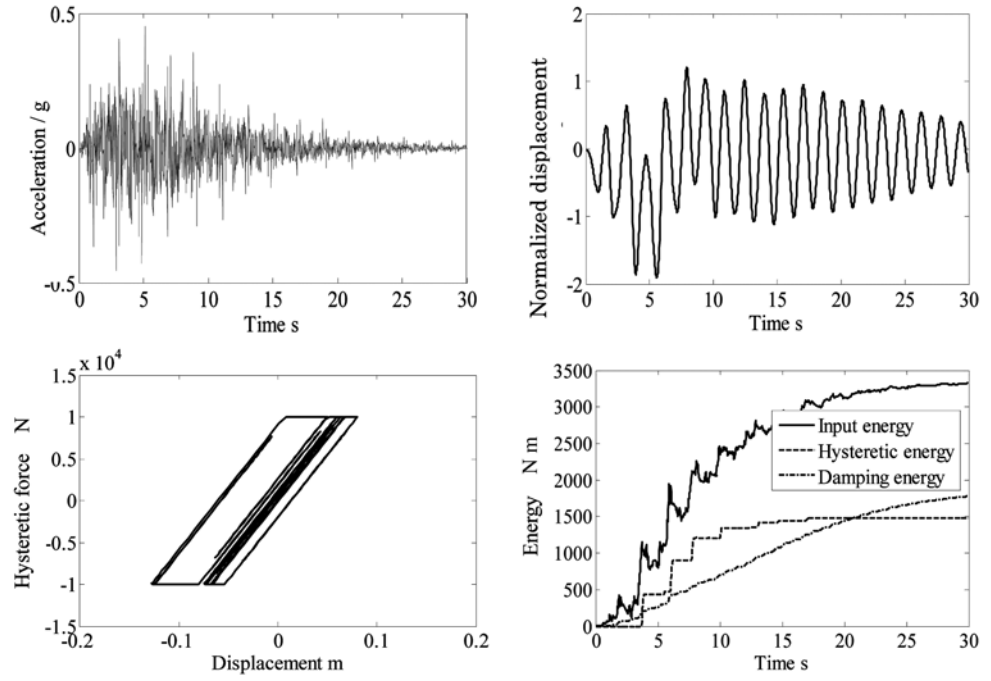

Fig. 8 Critical earthquake accelerations and associated critical responses for case 4

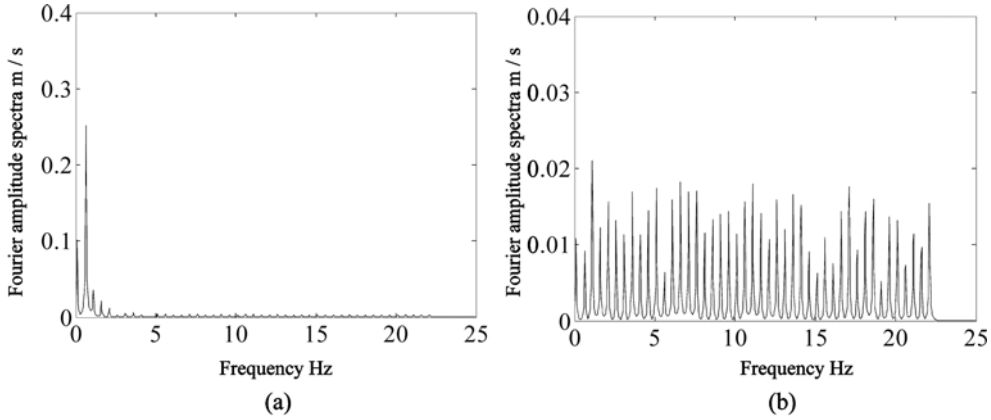

Fig. 9 Fourier amplitude of critical acceleration (a) case 1, (b) case 4

Table 3 Response parameters of SDOF (ω_n = 4.10 rad/s) to alternative acceleration inputs

Response quantity	Earthquake input load						
	El Centro NS record	Critical input (Model I)		Critical input (Model II)		Critical input (Model III)	
		Case 1	Case 2	Case 1	Case 2	Case 1	Case 4
Max. displ.* (m)	0.7518	1.1601	4.8370	2.04	3.85	-	-
Max. displ.** (m)	0.0918	0.0839	0.1653	0.1145	0.1655	0.16	0.13
Ductility	1.37	1.25	2.46	1.71	2.47	3.18	2.10
DI_{PA}	0.26	0.72	3.84	0.66	1.31	0.97	0.39

*Linear elastic analysis, **Elastic-plastic analysis

Table 4 Sensitivity analysis of the critical damage index to the constraints parameters

Parameter	E	M_1	M_2	M_3	$M_4(\omega)$	$M_5(\omega)$	α	β
ℓ_1	0.51	0.18	0.14	0.23*	0.16*	0.13	0.04	0.06
ℓ_2	4.52	1.60	1.71	2.04*	1.42*	1.15	0.36	0.53

*These values represent ℓ_1, ℓ_2 at the frequency at which $M_4(\omega)$, $M_5(\omega)$ reach their maximum values

The constraint scenarios considered in deriving critical earthquake inputs are listed in Table 2. The numerical results obtained are presented in Figs. 7-9 and Tables 3 and 4. Fig. 7 shows results for constraint scenario 1 and similar results for case 4 are shown in Fig. 8. Each figure shows the time history of the critical ground acceleration, the inelastic deformation, the hysteretic force and the energy dissipated by the structure. Based on extensive analyses of the numerical results, the following observations are made:

1. The frequency content and Fourier amplitude of the critical earthquake are strongly dependent on the constraints imposed (see Table 3). If available information on earthquake data is limited to the total energy and PGA, the critical input is resonant or of pulse-like nature and the structure deformation is conservative (see Fig. 7 and Table 3). Furthermore, most of the power

of the Fourier amplitude is concentrated at a frequency close to the natural frequency of the elastic structure while the amplitudes at other frequencies are low and uniformly distributed (see Fig. 9(a)). The results for case 1 match well with earlier works reported by Abbas (2006) and Takewaki (2001). These results, however, are substantially different from those for the elastic structure where all energy of the acceleration is centered around ω_0 (Abbas and Manohar 2002). Additional constraints on the Fourier amplitude spectra (see Table 3) force the Fourier amplitude of the critical acceleration to get distributed across other frequencies (see Fig. 9(b)). The critical acceleration possesses a dominant frequency that is close to the average frequency of past records. The realism of the critical earthquake input is also evident from the maximum damage index it produces. For instance, the damage index for case 4 is 0.39 (repairable damage) which is substantially smaller than 0.97 (damaged beyond repair) for case 1.

2. To investigate the influence of the damping ratio on the computed critical earthquake load, limited studies were carried out. The damping ratio is changed (namely, 0.01, 0.03 and 0.05) while all other parameters are kept unchanged. The critical earthquake is computed by solving a new optimization problem for each case. The value of the damping ratio is not seen to significantly influence the frequency content of the earthquake acceleration. It was observed, however, that the ductility ratio and the maximum inelastic deformation for the structure decrease for higher damping ratios. Thus, the ductility ratio decreases to 1.98 for the damping ratio of 0.05 while the ductility ratio increases to 2.95 for damping ratio = 0.01. It is also observed that the inelastic structure with higher damping ratio dissipates more energy through damping compared to that with lower damping ratio. The damage index also reduces when the damping ratio increases.
3. The sensitivity of the critical damage index with respect to variations in values of the constraints E, M_1, M_2, M_3, $M_4(\omega), M_5(\omega)$ and the envelope parameters α, β are studied using numerical methods. To examine the sensitivity of DI_{PA} with respect to a specific parameter, the value of this parameter is changed by 1% while all other parameters are held unchanged, and the optimization problem is solved again. This leads to the calculation of the percentage change in the optimal damage index ℓ_1, and also the ratio of change in the optimal DI_{PA} to the change in the parameter value ℓ_2. Table 4 summarizes the results of these calculations for case 4. For the bounds $M_4(\omega), M_5(\omega)$, the change of 1% is taken to be uniform across all frequencies. Table 4 reveals that the changes in energy E and PGD $M_4(\omega)$ alter the optimum solution considerably compared with similar changes in other parameters. The optimum solution is less sensitive to changes in the envelope parameters.

It may be emphasized that models I and II represent near-fault pulse-like ground motions with an equivalent main pulse. Model III, however, accounts for the multi-pulses in the ground velocity. As is well known, this class of ground motion may contain several pulses. Moreover, the ground motion has been treated as being deterministic in nature. The modeling of this class of ground motion using the probabilistic approach facilitates handing uncertainties in the ground motion, variability in the structure's parameters and assessing the structure's reliability. These aspects have been recently investigated by the present authors (Moustafa and Takewaki 2010). Furthermore, the reduction of the structural responses under strong ground motion using passive dampers has also been studied (Takewaki 2009, Fujita *et al.* 2010).

5. Conclusions

This paper investigated the distinctive features of near-fault pulse-like ground motions. These ground motions are characterized using measures based on analyses of the earthquake records. In this paper, a new measure for characterizing the effective frequency content of the ground acceleration has also been developed. An additional measure for the frequency content of the ground motion based on the work of Vanmarcke (1972, 1976) has also been examined. It has been shown that both measures successfully identify resonant or pulse-like ground motions. The energy rate of the ground acceleration in time and frequency domains were also employed for the same purpose. Pulse-like ground motions have also been characterized in terms of measures of the structural performance during the ground shaking (e.g., response, energy and damage spectra). The paper provides also simple analytical models for this class of ground motion which can be used by the structural engineer to assess the safety of linear structures without the need for numerical integration of the equations of motion.

Given the central importance of considering nonlinear behavior of structures in earthquake engineering, the mathematical modeling of near-fault pulse-like ground motions has also been investigated for inelastic structures using the critical excitation method combined with optimization techniques and damage indices. It has been shown that the method can successfully model pulse-like or resonant ground motions at sites having limited earthquake data.

Acknowledgements

This research work is partly supported by funds from the Japanese Society for the Promotion of Science. The support is gratefully acknowledged. The authors thank two anonymous reviewers for careful reading of the paper and insightful comments they made.

References

Abbas, A.M. (2006), "Critical seismic load inputs for simple inelastic structures", *J. Sound Vib.,* **296**, 949-967.

Abbas, A.M. and Manohar, C.S. (2002), "Investigations into critical earthquake load models within deterministic and probabilistic frameworks", *Earthq. Eng. Struct. D.,* **31**, 813-832.

Abbas, A.M. and Manohar, C.S. (2007), "Reliability-based vector nonstationary random critical earthquake excitations for parametrically excited systems", *Struct. Saf.,* **29**, 32-48.

Akiyama, H. (1985), *Earthquake-resistant Limit-state Design for Buildings*, University of Tokyo Press, Tokyo.

Anderson, J. and Bertero, V. (1987), "Uncertainties in establishing design earthquakes", *J. Struct. Eng-ASCE*, **113**(8), 1709-1724.

Arias, A. (1970), *A Measure of Earthquake Intensity: Seismic Design of Nuclear Power Plants*, MIT press, Cambridge.

Arora, J.S. (2004), *Introduction to Optimum Design*, Elsevier Academic Press, San Diego.

Bray, J.D. and Rodriguez-Marek, A. (2004), "Characterization of forward-directivity ground motions in the near-fault region", *Soil Dyn. Earthq. Eng.,* **24**, 815-828.

Caleman, T., Branch, M.A. and Grace, A. (1999), *Optimization Toolbox for the Use with Matlab, User's Guide*, The Math Works Inc., USA.

Chai, Y.H. and Fajfar, P. (2000), "A procedure for estimating input energy spectra for seismic design", *J. Earthq. Eng.,* **4**(4), 39-561.

Cosenza, C., Manfredi, G. and Ramasco, R. (1993), "The use of damage functionals in earthquake engineering: a comparison between different methods", *Earthq. Eng. Struct. D.,* **22**, 855-868.
Fujita, K., Moustafa, A. and Takewaki, I. (2010), "Optimal placement of viscoelastic dampers and supporting members under variable critical excitations", *Earthq. Struct.*, **1**(1), 43-67.
Ghobara, A., Abou-Elfath, H. and Biddah, A. (1999), "Response-based damage assessment of structures", *Earthq. Eng. Struct. D.,* **28**, 79-104.
Hall, J.H., Heaton, T.H., Halling, M.W. and Wald, D.J. (1995), "Near-source ground motion and its effect on flexible buildings", *Earthq. Spectra,* **11**, 569-605.
He, W.L. and Agrawal, A.K. (2008), "Analytical model of ground motion pulses for the design and assessment of seismic protective systems", *J. Struct. Eng-ASCE,* **134**(7), 1177-1188.
Heaton, T.H., Hall, J.H., Wald, D.J. and Halling, M.W. (1995), "Response of high-rise and base-isolated buildings in a hypothetical MW 7·0 blind thrust earthquake", *Science,* **267**, 206-211.
Hough, S.E. and Bilham, R.G. (2006), *After the Earth Quakes: Elastic Rebound on an Urban Planet*, Oxford University Press, NY.
Housner, G.W. and Hudson, D.E. (1958), "The Port Hueneme earthquake of March 18, 1957", *B. Seismol. Soc. Am.*, **48**(2), 163-168.
Housner, G.W. (1970), *Strong Ground Motion*: *Earthquake engineering*, (Ed. Wiegel, R.L.), Prentice Hall, NJ.
Housner, G.W. and Trifunac, M.D. (1967), "Analysis of accelerograms-Parkfield earthquake", *B. Seismol. Soc. Am.*, **57**(6), 1193-1220.
Housner, G.W. and Jennings, P.C. (1977), "The capacity of extreme earthquake motions to damage structures", *Structural and Geotechnical Mechanics*, A volume honoring N.M. Newmark, Prentice-Hall Englewood Cliff, 102-116.
Makris, N. (1997), "Rigidity-plasticity-viscosity: Can electrorheological dampers protect base-isolated structures from near-source ground motions?", *Earthq. Eng. Struct. D.,* **26**, 571-591.
Moustafa, A. (2009), "Critical earthquake load inputs for multi-degree-of-freedom inelastic structures", *J. Sound Vib.*, **325**(3), 532-544.
Moustafa, A. (2010), "Discussion of analytical model of ground motion pulses for the design and assessment of seismic protective systems", *J. Struct. Eng-ASCE*, **136**(2), 229-230.
Moustafa, A. and Takewaki, I. (2010), "Deterministic and probabilistic representation of near-field pulse-like ground motion", *Soil Dyn. Earthq. Eng.*, **30**(5), 412-422.
Pacific Earthquake Engineering Research Center (2005), http://peer.berkeley.edu
Park, Y.J., Ang, A.H.S. and Wen, Y.K. (1985), "Seismic damage analysis of reinforced concrete buildings", *J. Struct. Eng-ASCE,* **111**(4), 740-757.
Powell, G.H. and Allahabadi, R. (1988), "Seismic damage predictions by deterministic methods: concepts and procedures", *Earthq. Eng. Struct. D.,* **16**, 719-734.
Shinozuka, M. (1970), "Maximum structural response to seismic excitations", *J. Eng. Mech.,* **96**, 729-738.
Takewaki, I. (2001), "Probabilistic critical excitation for MDOF elastic-plastic structures on compliant ground", *Earthq. Eng. Struct. D,* **30**, 1345-1360.
Takewaki, I. (2002), "Seismic critical excitation method for robust design: A review", *J. Struct. Eng-ASCE,* **128**, 665-672.
Takewaki, I. (2004), "Bound of earthquake input energy", *J. Struct. Eng-ASCE*, **130**, 1289-1297.
Takewaki, I. (2006), "Probabilistic critical excitation method for earthquake energy input rate", *J. Eng. Mech.,* **132**(9), 990-1000.
Takewaki, I. (2007), *Critical Excitation Methods in Earthquake Engineering,* Elsevier, Amsterdam.
Takewaki, I. (2009), *Building Control with Passive Dampers: Optimal Performance-based Design for Earthquakes*, John Wiley & Sons (Asia), Singapore.
Tan, P., Agrawal, A.K. and Pan, Y. (2005), "Near-field effects on seismically excited highway bridge equipped with nonlinear viscous dampers", *Bridge Struct.,* **1**(3), 307-318.
Trifunac, M.D. (2005), "Power design method", *Proceedings of Earthquake Engineering in the 21st Century to Mark 40th Anniversary of IZIIS*-Skopje, Macedonia, Skopje and Ohrid, August.
Trifunac, M.D. (2008), "Energy of strong motion at earthquake source", *Soil Dyn. Earthq. Eng.*, **28**, 1-6.
Trifunac, M.D. and Brady, A.G. (1975), "A study on the duration of strong earthquake ground motion", *B.*

Seismol. Soc. Am., **65**(3), 581-626.
Uang, C.M. and Bertero, V.V. (1990), "Evaluation of seismic energy in structures", *Earthq. Eng. Struct. D.,* **19**, 77-90.
Vanmarcke, E.H. (1972), "Properties of spectral moments with applications to random processes", *J. Eng. Mech.,* **42**, 215-220.
Vanmarcke, E.H. (1976), *Structural Response to Earthquakes*: *Seismic Risk and Engineering Decisions*, (Eds. Lomnitz, C. and Rosenbluth, E.), Elsevier, NY.
Zhang, J. and Makris, N. (2001), "Rocking of free-standing blocks under cycloidal pulses", *J. Eng. Mech.*, **127**(5), 473-483.
Zahrah, T.F. and Hall, W.J. (1984), "Earthquake energy absorption in sdof structures", *J. Struct. Eng-ASCE*, **110**, 1757-1772.